Geodesic domes for planetary exploration

Research Article

Enrico Ossola*, Eugenio Brusa, and Raffaella Sesana

Geodesic domes for planetary exploration

https://doi.org/10.1515/cls-2020-0018
Received Sep 24, 2020; accepted Oct 27, 2020

Abstract: Venus and the Ocean Worlds are emerging areas of interest for space exploration, as they can potentially host, or have hosted, conditions compatible with life. Landers and probes for in-situ exploration, however, must deal with very high external pressure, due to the environmental conditions, often resulting in thick and heavy structures. Robust, reinforced shell structures can provide a lightweight solution for the primary structure. In this frame, the isogrid layout is already a standard in aerospace, especially for flat panels or cylindrical shells. In this paper, isogrid-stiffened hemispherical shells, or "geodesic domes", are described, focusing on the case of a concept of a Venus lander. Early design methods for both plain and geodesic domes subjected to external pressure are presented, providing design equations. Additive Manufacturing is identified as the key technology for fabricating metallic geodesic domes, due to the complexity of the internal features. Moreover, it allows to fabricate ports and integrated thermostructural systems in the same process, potentially resulting in improved performance or cost and schedule savings.

Keywords: isogrid structures, additive manufacturing, buckling, knockdown factor

1 Introduction

In the last decades, new discoveries in planetary science have turn the spotlight on a series of planets and moons, characterized by internal oceans and potentially hosting life, such as Europa or Enceladus. Mission concepts are currently under study, aimed to land on the surface and penetrate into the crust, attempting in situ life detection [1]. Searching for water, another interesting target is Venus. Very similar to Earth in structure and size, it is thought to host oceans in the past; however, a severe greenhouse effect has made its atmosphere inhabitable today. Several concepts for atmospheric and surface missions have been proposed or are currently under study [2].

Both the Ocean Worlds and Venus are characterized by harsh environmental conditions, such as very high external pressure, extreme temperature and corrosive environment. In the case of Venus, 93 bar and 462°C are expected at the surface, posing challenging conditions for the structural and the thermal control system of surface probes. Spherical shells are one of the preferred options for the primary structure, because of the high internal volume to surface ratio. Past robotic missions to Venus, for example, used plain spherical shells, composed by 2 or 3 parts assembled together.

Internal ribbing, although difficult and expensive to fabricate with traditional manufacturing techniques, could help in increasing the bending stiffness of the shell, resulting in significant mass savings. In this frame, plates and shells stiffened with ribs forming a triangular pattern are commonly referred as "isogrids". Metallic or composite isogrid panels are largely used for aerospace applications, where stiff and light structures are needed. Spherical isogrid shells are quite rare in aerospace, but are very common in architecture, as geodesic domes. They are usually composed by a metal or wooden framework covered by polymeric, glass or plywood panels. Due to the resource efficiency and the ease of fabrication and deployment, geodesic domes have been used for a number of applications, ranging from military shelters, to radar equipments, biospheres or large auditoriums [3]. Concepts for lighter-than-air structures with an isogrid or icosahedral layout have been recently proposed in [4, 5]. In the case of geodesic domes for robotic space probes, the fabrication issues related to the complex internal ribbing can be easily addressed by using Additive Manufacturing (AM) technologies. AM geodesic domes could potentially be applied not only to space probes for planetary exploration, but also to manned or unmanned underwater vehicles [6, 7], pressure hulls [8], components for vacuum systems [9] or

Article note: Paper included in the Special Issue entitled: Shell and Spatial Structures: Between New Developments and Historical Aspects

***Corresponding Author: Enrico Ossola:** Department of Mechanical and Aerospace Engineering, Politenico di Torino, Italy. Visiting Student at Jet Propulsion Laboratory, California Institute of Technology, Pasadena, California; Email: enrico.ossola@polito.it
Eugenio Brusa, Raffaella Sesana: Department of Mechanical and Aerospace Engineering, Politenico di Torino, Torino, Italy

underwater structures [10], where plain spheres are currently used.

Aim of this work is proposing a design approach for Additively Manufactured metallic geodesic domes undergoing external pressure. First, plain spherical shells will be analyzed, describing one of the most used design formulas for buckling sensitive shells. Then, geodesic domes and isogrid layouts will be introduced, summarizing the main analytical formulation and describing a methodology to design external pressure vessels. Finally, some results of a preliminary experimental campaign performed on Additive Manufactured geodesic domes will be presented as well.

2 Traditional design: plain shells

2.1 State of stress

Consider a spherical vessel of radius R subjected to a uniform external pressure p_{ext}, as shown in Figure 1. A spherical coordinate system $\{\vec{r}, \vec{\theta}, \vec{\phi}\}$ can be defined so that the external pressure is applied along the radial direction. $\sigma_r, \sigma_\theta, \sigma_\phi$ and $\epsilon_r, \epsilon_\theta, \epsilon_\phi$ are respectively stress and strain along the three directions. Due to the symmetry in geometry and loading conditions, $\{\vec{r}, \vec{\theta}, \vec{\phi}\}$ are principal directions and the behavior in azimuthal ($\vec{\theta}$) and polar direction ($\vec{\phi}$) are equivalent.

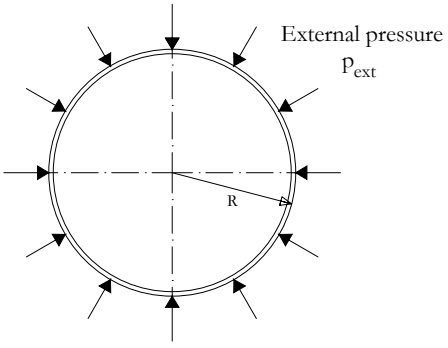

Figure 1: Scheme of the problem

If the wall thickness t is less then 1/10 of the radius, the radial stress due to the external pressure is negligible if compared to the tangential stress. Being the sphere made of a material with Young's modulus E and Poisson's ratio ν, the state of stress can be described as follows:

$$\begin{cases} \sigma_r \approx 0 \\ \sigma_\theta = -\dfrac{p \cdot \pi R^2}{2\pi R t} = -\dfrac{pR}{2t} \\ \sigma_\phi = \sigma_\theta \end{cases} \tag{1}$$

Given isotropic material properties, it is possible to obtain the strains, as:

$$\begin{cases} \epsilon_r = -\dfrac{2\nu}{E}\sigma_\theta \\ \epsilon_\theta = \epsilon\phi = \dfrac{1-\nu}{E}\sigma_\theta \end{cases} \tag{2}$$

and finally the radial displacement u_r:

$$\epsilon_\theta = \frac{2\pi(r+u_r) - 2\pi r}{2\pi r} = \frac{u_r}{r} \Rightarrow u_r = \epsilon_\theta \cdot r \tag{3}$$

2.2 Structural stability

In addition to yielding, the system is prone to fail because of structural instability as well. In fact, thin spherical shells are characterized by high membrane stiffness, but low bending stiffness; so, they can withstand high pressure loads in static conditions, but catastrophic failures are possible if a load or geometry perturbation occurs, inducing bending phenomena [11]. The buckling behavior of a complete and ideal spherical shell subjected to uniform external pressure was firstly studied by Zoelly in 1915 [12], who obtained the "classical" formulation reported below:

$$p_{cl} = \frac{2E}{\sqrt{3 \cdot (1-\nu^2)}} \frac{t^2}{R^2} \tag{4}$$

Since this early study, a large difference between the theoretical critical pressure and the experimental evidences was observed. The cause of this discrepancy was identified in the high sensitivity of thin spherical shells to geometrical, material and loading imperfections. For this reason, the actual critical pressure (p_{cr}) is calculated by modifying the ideal critical pressure p_{cl} (Eq. 4) applying a knockdown factor KF, in order to take into account the detrimental effect of imperfections.

$$p_{cr} = \mathrm{KF} \cdot p_{cl} \tag{5}$$

The KF value is derived from experimental tests and depends on shape and size of the component. One of the main issues in spherical shell buckling is the high scattering of the knockdown factor [12, 13]. Figure 2 summarizes the experimental results of some researches. In general, a

decrease in KF value is observed when the ratio R/t gets bigger; indeed, larger and thinner shells are more likely subjected to deviations from the perfect geometry because of the fabrication process, and non uniform loading and boundary conditions are more probable.

Lee *et al.* [12], producing and testing almost-perfect elastomeric spherical shells, obtained higher and less scattered values of KF, ranging from 0.61 to 0.92. At the same time, they studied the effect of geometric imperfections, precisely fabricating dimp-like defects on the shells.

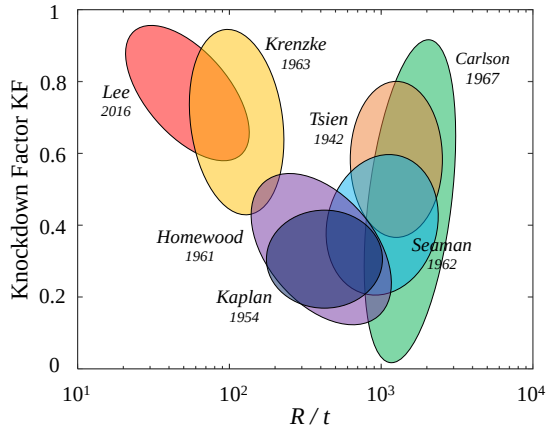

Figure 2: Knockdown factor versus radius to thickness ratio: experimental results from the literature (adapted from [12]).

The high variability of the experimental results is reflected on the KF values to use in the design stage, ranging from 14% [14], to 30% [15] and above. NASA SP8032 [14] reports recommended KF values for both spheres and spherical caps. As it is possible to see from Figure 3, the KF is a function of the geometry parameter λ_{geom}, which depends on the R/t ratio and on the included angle of the cap Φ (sphere: $\sin\Phi = 0$). When the ratio R/t increases, the buckling resistance decreases asymptotically to 0.14. A less conservative value was used in the Pioneer mission (KF = 40%). This approach was possible because an extensive experimental campaign proved the high buckling resistance of that particular geometry.

In the design stage, different assumptions on the required KF value can lead to very different designs, as shown in Figure 4, where the critical buckling pressure p_{cr} is plotted against the shell thickness using different KFs, considering a R=100 mm spherical shell made of Ti6Al4V. For instance, considering a design pressure of 300 bar (dotted line), the required shell thickness is 2.7 or 4 mm, if a KF of 14% or 30% is applied. It is clear that a deep investigation on the correct value of KF is crucial, to optimize a structure, given the geometry, the size and the manufacturing technique.

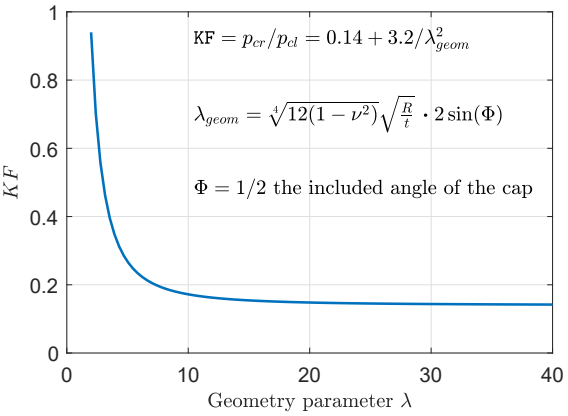

Figure 3: NASA SP-8032 - recommended KF for spherical caps [14]

More complex analytical formulations have been proposed [12, 16–18], but the Zoelly's equation is still largely used in the early design stage for its ease of use.

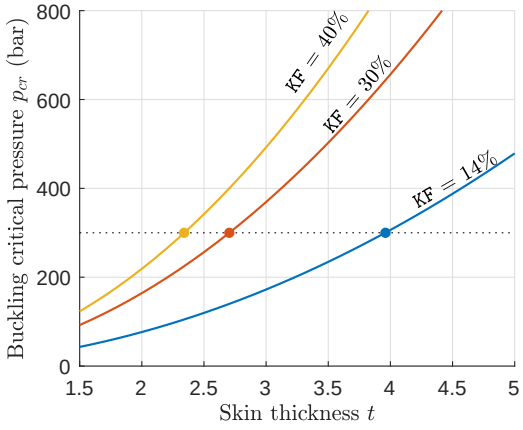

Figure 4: Bucking critical pressure against shell thickness, considering a range of KF, from 14% to 40%

2.3 Finite Element Analysis

Buckling problems can be addressed with a numerical approach as well. Several different methods are available, starting from the Linear Bifurcation Analysis (LBA). In the case of thin spherical shell, the results of LBA are in agreement with Zoelly's equation (*i.e.* when KF = 1). More sophisticated tools have been developed as well, in order to take into account the effects of material and geometric non linearities and to simulate imperfections. An outline of de-

sign procedures using non linear analysis is reported by Rotter [19], based on the European Standard code EN-1993-1-6 [20]. Sensitivity of spherical shells to imperfections has been investigated using material non linear analysis in [8] and in [21]; the first one analyzed large pressure hulls (R=1000 mm) using both linear and non linear methods, simulating a range of defects and proposing an empirical formula for estimating the actual critical pressure. Combined loading cases, like external pressure together with circumferential shear, have been investigated by Tall *et al.* [22].

2.4 Manufacturing techniques

Depending on the material, the size of the component and on the required level of precision, different manufacturing techniques are available [23]. Large, metallic hemispheres can be obtained by spin forming and eventually post-machining if higher accuracy is required. Spin forming, however, is not possible in case of brittle materials, like beryllium, so they need to be machined from billets, resulting in high manufacturing costs and time. Composite cylindrical tank are usually obtained by wrapping, but hemispherical shapes may be more difficult to fabricate. Sandwich pressure vessels can be fabricated by bulge-forming the different parts and then assembling them. High precision plastic domes can be obtained by vacuum drawing [12].

3 Geodesic domes for harsh environments

3.1 The isogrid layout

Isogrid structures consist of panels or shells stiffened with a system of ribs arranged in a triangular pattern, as shown in Figure 5. The ribs are oriented and spaced so that they form equilateral triangle; this, macroscopically, lead to an isotropic behavior. Isogrid structures show high mechanical strength and bending stiffness, but low mass. For this reason, they are widely used in aerospace applications, such as cylinders for launch vehicles. Different rib geometries and materials have been investigated, ranging from metal to plastic, to composites [24]. Bellifante and Meyer [25] and the "Isogrid Design Handbook" [26] are the main references for analytical models for isogrid structures.

3.2 Stress state of an Isogrid panel

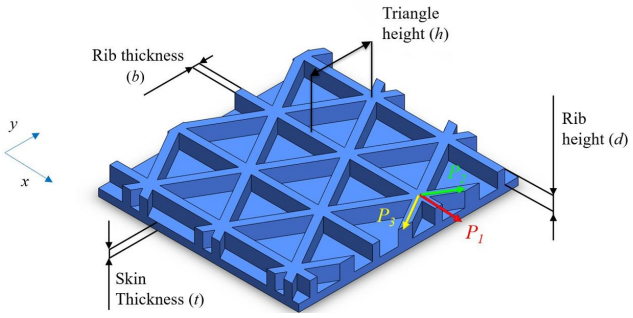

Figure 5: Isogrid geometry

This section reports the main formulas for stress state calculation from [26]. Figure 5 shows the top view and the section of a typical isogrid structure. A global $\{x, y\}$ and a local $\{P_1, P_2, P_3\}$ reference frame are defined and used for describing stress resultant and rib stresses respectively, despite the usual symbols applied in the literature, which resorts to 1, 2, 3 to indicate the principal system of reference. The isogrid geometry (skin thickness t, rib thickness b, rib height d, triangle height h) is highlighted in Figure 5.

Non dimensional parameters related to the geometry are defined as follows:

$$\alpha = \frac{bd}{th} \tag{6a}$$

$$\delta = \frac{d}{t} \tag{6b}$$

$$\beta = \sqrt{3\alpha(1+\delta)^2 + (1+\alpha)(1+\alpha\delta^2)} \tag{6c}$$

and used to calculate the equivalent area A and moment of inertia I per unit of triangle height:

$$A = t \cdot (1+\alpha) \tag{7a}$$

$$I = \frac{t^3}{12} \cdot \frac{\beta^2}{1+\alpha} \tag{7b}$$

and the extensional (K) and bending (D) stiffnesses:

$$K = \frac{Et}{1-\nu^2} \cdot (1+\alpha) \tag{8a}$$

$$D = \frac{Et^3}{12(1-\nu^2)} \cdot \frac{\beta^2}{1+\alpha} \tag{8b}$$

where the first factors represent the formulas for the skin alone, while the second ones are the corrections for the isogrid.

Using eq.8, it is possible to define an equivalent monocoque thickness (t_e) and Young's modulus (E_e) as follows:

$$\begin{cases} K = \dfrac{E_e t_e}{1-\nu^2} \\ D = \dfrac{E_e t_e^3}{12(1-\nu^2)} \end{cases} \Rightarrow \begin{cases} t_e = t\dfrac{\beta}{1+\alpha} \\ E_e = E\dfrac{(1+\alpha)^2}{\beta} \end{cases} \tag{9}$$

These expressions are used to evaluate stress resultants and buckling critical pressures.
When the bending stresses are negligible, stress state of skin and ribs can be expressed by eq.10 and eq.11 respectively, where N is the load per unit of length:

$$\begin{cases} \sigma_x = \dfrac{1}{t(1+\alpha)} N_x \\ \sigma_y = \dfrac{1}{t(1+\alpha)} N_y \\ \tau_{xy} = \dfrac{1}{t(1+\alpha)} N_{xy} \end{cases} \tag{10}$$

$$\begin{cases} \sigma_1 = \dfrac{1}{3t(1+\alpha)}(3N_x - N_y) \\ \sigma_2 = \dfrac{2}{3t(1+\alpha)}(N_y + \sqrt{3}N_{xy}) \\ \sigma_3 = \dfrac{2}{3t(1+\alpha)}(N_y + \sqrt{3}N_{xy}) \end{cases} \tag{11}$$

3.3 Geodesic domes

The layout of isogrid spherical shells (or icospheres) is obtained starting from the regular icosahedron. As shown in Figure 6, this polyhedron is composed by 20 equal equilateral triangular faces, whose vertices lay according to Table 1.

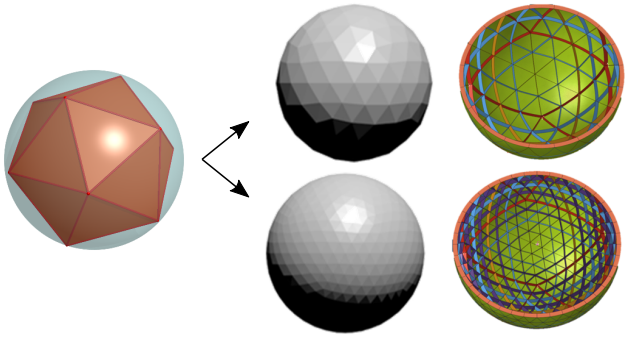

Figure 6: Icoshaderon and geodesic domes with two different isogrid frequencies

The icosphere is obtained by projecting the edges of the icosahedron on the spherical surface and then creating the ribs. Isogrid frequency (*i.e.* triangle height h) can be varied by subdividing the triangular faces in smaller triangles. Defining the number of subdivisions as n_{div}, the triangle height is calculated as:

Table 1: Icoshahedron vertices, according to a rectangular reference frame. $\phi = (1+\sqrt{5})/2 \approx 1.618$

A =	$(0, 1, \phi)$	E =	$(\phi, 0, 1)$	I =	$(1, \phi, 0)$
B =	$(0, -1, \phi)$	F =	$(\phi, 0, -1)$	J =	$(-1, \phi, 0)$
C =	$(0, -1, -\phi)$	G =	$(-\phi, 0, -1)$	K =	$(-1, -\phi, 0)$
D =	$(0, 1, -\phi)$	H =	$(-\phi, 0, 1)$	L =	$(1, -\phi, 0)$

$$h_T = \frac{\sqrt{3}}{2} \cdot \frac{2\pi R}{10 \cdot 2^{n_{div}-1}} \tag{12}$$

It must be noted that the triangular cells obtained by the projection on the sphere are not regular and different each other, although the original icosahedron has 20 equal equilateral triangles. In the following, the value of h is related to the to the height of the triangle in correspondence to the center of each of the 20 faces of the original icosahedron. Figure 6 reports isogrid layout for 2 and 3 subdivisions.

3.4 Analytical modeling

The stress state of a geodesic dome under uniform external pressure can be calculated starting from Eq. 10 and 11, considering that:

$$\begin{cases} N_x = N_y = pR/2 \\ N_{xy} = 0 \end{cases} \tag{13}$$

Therefore, the stress in the skin and in the ribs can be written as follows:

$$\sigma_{\theta,\phi}^{skin} = \frac{pR}{2t(1+\alpha)} \tag{14a}$$

$$\sigma_{1,2,3}^{rib} = \frac{pR}{3t(1+\alpha)} \tag{14b}$$

Similarly to the plain shell case, the structural instability needs to be investigated as well. An analytical formulation based on [26] is reported in this section. Because of the complexity of the structure, three different buckling modes can occur, involving the General Instability (GI) of the whole system, the Skin Buckling (SB) of the shell within the triangular pockets, or the Rib Crippling (RC).

Starting from the Zoelly's formula for plain spheres (Eq. 4), the General Instability equation can be obtained by replacing the Young's modulus and the thickness with

the equivalent parameters calculated using Eq. 9, in order to take into account the contribution of the ribs.

$$p_{cl} = \frac{2E_e}{\sqrt{3(1-\nu^2)}}\frac{t_e^2}{R^2} = \frac{2E}{\sqrt{3(1-\nu^2)}}\frac{t^2}{R^2}\beta \tag{15}$$

A KF is finally applied and the formula is written according to the nomenclature used in [26]:

$$p_{\mathrm{GI}} = \frac{\mathrm{KF}}{\sqrt{3(1-\nu^2)}} \cdot 2E\frac{t^2}{R^2}\beta = c_0 \cdot 2E\frac{t^2}{R^2}\beta \tag{16}$$

The parameter c_0 needs to be found empirically. According to the experimental campaign on plastic and aluminum domes performed in [25], c_0 is set to 0.26. It must be noted that the reference dates back to the 1960s and only a few number of specimens were tested; further experimental campaigns should be performed, considering current technologies.

The second type of instability concerns the skin only. At this stage, the curvature of the triangular elements is neglected. The buckling behavior of flat and curved shells can differ, but this assumption is reasonable in case of large spheres and small triangular cells and it allows to use a simplified analytical model. A planar triangle, hinged on the three edges and loaded is considered, as shown in Figure 7a. The skin buckling critical pressure can be calculated by equating the buckling critical stress for equilateral triangular plates (with $k_1 = 5$) to the skin stress (Eq. 14a):

$$\frac{k_1\pi^2 E}{12(1-\nu^2)}\left(\frac{t}{\sqrt{3}/2h}\right)^2 = \frac{p_{\mathrm{SB}}R}{2t(1+\alpha)} \tag{17}$$

The ribs can be modeled as rectangular plates (neglecting the curvature), hinged on 3 edges an loaded on the two opposite short edges (see Figure 7, b); the corresponding buckling critical stress is evaluated as follows ($k_2 = 0.456$):

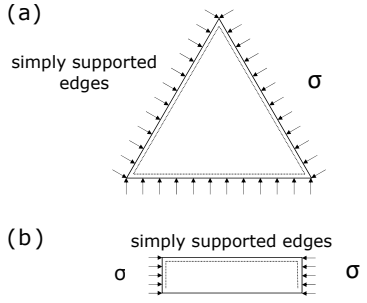

Figure 7: Scheme of skin buckling (a) and rib crippling (b) - adapted from [25]

$$\frac{k_2\pi^2 E}{12(1-\nu^2)}\left(\frac{b}{d}\right)^2 = \frac{p_{\mathrm{RC}}R}{3t(1+\alpha)} \tag{18}$$

The following equations summarize the formulas for structural instability:

$$p_{\mathrm{GI}} = c_0 \cdot 2E \cdot \frac{t^2}{R^2}\beta\,; \qquad c_0 = 0.26 \tag{19a}$$

$$p_{\mathrm{SB}} = c_1 \cdot 2E \cdot \frac{t(1+\alpha)}{R}\frac{t^2}{h^2}\,; \qquad c_1 = 3.47 \tag{19b}$$

$$p_{\mathrm{RC}} = c_2 \cdot 2E \cdot \frac{t(1+\alpha)}{R}\frac{b^2}{d^2}\,; \qquad c_2 = 0.634 \tag{19c}$$

3.5 Structural optimization

A Matlab® code for designing geodesic spheres undergoing external pressure loading was developed, starting from the analytical formulation given in [26]. Given the sphere radius, the material properties and the external pressure, the isogrid layout (*i.e.* skin thickness, rib height and thickness) needs to be optimized, in order to minimize the mass, given the required safety factors for yielding and buckling. The non dimensional parameter λ is defined as follows:

$$\lambda = \frac{p_{cr}}{p_{ext}} \tag{20}$$

Being three the buckling modes and the relative critical pressures (GI, SB, RC), three different values of λ can be calculated. According to [26], the optimum structure is obtained by equating the three buckling equations:

$$\lambda_{\mathrm{GI}} = \lambda_{\mathrm{SB}} = \lambda_{\mathrm{RC}} \Rightarrow optimum \tag{21}$$

In this way, the three buckling phenomena should occur at the same time, when the critical pressure is reached. The stress state must be always checked as well, in order to avoid a yielding failure. The validity of Eq. 21 will be discussed in the following.

The isogrid layout is described by 4 parameters: h, t, b and d. It must be noted that the triangle height h can be easily controlled, as it can vary discretely only, depending on the number of subdivisions of the original icosahedron. For this reason, it was decided to exclude it from the optimization problem. In other terms, given an isogrid frequency (*i.e.* given h), an optimization problem will be solved. Multiple configurations, having bigger or smaller triangles, can be finally compared.

Excluding h allows to reduce the design variables to three parameters only (t, b and d). Equating SB and RC

equations (19), *i.e.* imposing that the two failure modes occur simultaneously, the rib height d can be written as function of skin and rib thickness:

$$d = \frac{bt}{h}\sqrt{\frac{c_2}{c_1}} \Rightarrow \lambda_{SB} = \lambda_{RC} \tag{22}$$

Now, given the sphere radius, the number of subdivisions, the material properties and the external pressure, it is possible to map the λ values as a function of skin thickness t and rib thickness b only (see Figure 8). Skin buckling and Rib crippling plots are exactly the same, as imposed by Eq. 22. The curves intersect in series of optimum points, in yellow. The top view of the plot can be finally used to easily find the optimum geometry, as shown in Figure 9, which shows not only the optimum curve (in yellow), but also the level curves relative to the rib height d (in purple) and to the minimum buckling pressure (in red), and the mass color plot (background). The design point can be obtained by the intersection between the required minimum critical pressure and the optimum curve. The isogrid geometric parameters (t, b, and d) are read from the plot, as well as the corresponding mass. Finally, the solution needs to be verified for yielding.

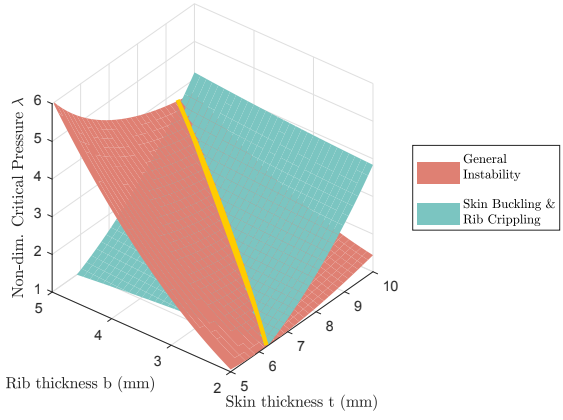

Figure 8: Intersection between the buckling modes for different values of skin and rib thickness

Eq. 21 is checked, in order to verify that this condition results in a configuration of minimum mass. A R=560 mm, Ti6Al4V geodesic sphere is designed with a design pressure of 150 bar. The optimum point is found by using the procedure previously described, resulting in a mass of 184 kg. Then, the isogrid configuration is modified, keeping the same mass. Three plots are obtained 10 , by varying two of the three isogrid design parameters (t, d and b) and keeping constant the third one. As it is possible to see, the point found assuming Eq. 21 is actually an optimum point,

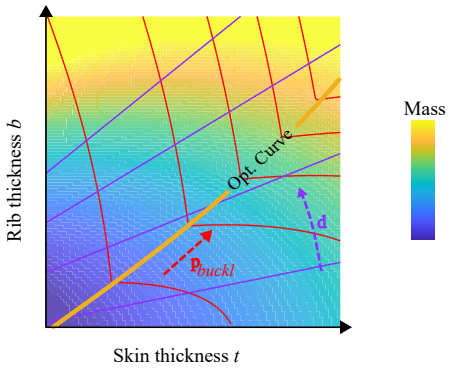

Figure 9: Optimum geometry plot

at least locally. For instance, when d = const (first plot), moving from left to right means having thicker ribs and thinner ribs, *i.e.* going from a rib crippling sensitive structure, to a skin buckling sensitive structure, going through an optimum point. Similar considerations are applicable to the other two plots.

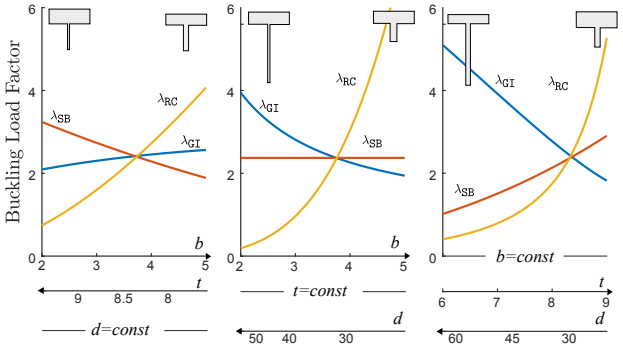

Figure 10: Optimum design point

3.6 Finite Element Analysis

Finite Element Method can be used to numerically estimate the stress state and the buckling critical load of geodesic domes subject to external pressure. Due to the particular geometry, the mesh creation process can be complex. A procedure for creating the mesh is briefly reported, using Altair HyperWorks® as the preprocessor and Altair Optistruct® as the solver.

First, the icosahedron is created, by manually inputting the coordinates given in Table 1. One face of the icosahedron out of the 20 is then projected the circumscribing spherical surface and divided in smaller triangles. Then, surfaces for the ribs are created and the geometry is meshed. In this case, ≈ 7800 quadrangular elements have

been used. Then, a Matlab® script is used to create all the 20 faces of the icosahedron, by replicating the elements previously created. Finally, duplicated nodes are merged and a cylindrical global system of reference is assigned to all the nodes. Symmetry conditions are finally applied to the nodes on the symmetry plane (xy plane), allowing only radial translation and z rotation. A uniform external pressure is applied normally to the outer surface (Figure 11).

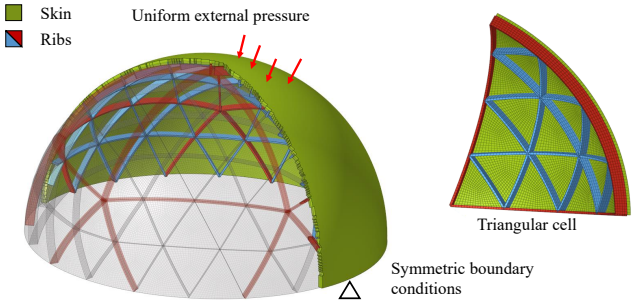

Figure 11: Model for FEA

Linear static analysis and linear buckling analysis can finally be run. In the latter case, it is possible not only to estimate the buckling pressure, but also to identify the type of buckling (general instability, skin buckling or rib crippling), as shown in Figure 12. Linear FEA and analytical methods are compared, by computing stress state and buckling pressure in a number of different geometries, as shown in Table 2. Three sets of experiments are run; for each set, h and d are constant and a 7x7 design is generated, considering changes of t and b equal to ±50%, ±25%, and ±12.5% in respect to the nominal value.

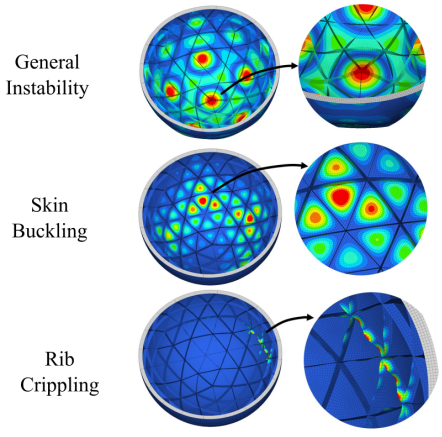

Figure 12: FEA Post-precessing: examples of different buckling modes. From left to right: `GI`, `SB` and `RC`

Table 2: Set of trail cases for FEM/analytical method comparison

		set 1	set 2	set 3
h	(mm)	157	157	79
d	(mm)	30	60	30
t_{nom}	(mm)	8.40	14.70	5.00
b_{nom}	(mm)	3.80	3.10	4.50

Figure 13 shows the values of non dimensional critical loads computed analytically and numerically; as it is possible to see, a discrepancy in buckling critical pressures is observed. The slope of the regression line is equal to 0.57, 0.60 and 0.55 in the three sets of simulations. It must be noticed that analytical and FEM results are in agreement for plain spheres, when Zoelly's classical equation 4 is used (`KF` = 1). The difference can be related to the adoption of the suggested `KF` in the `GI` equation (Eq. 19).

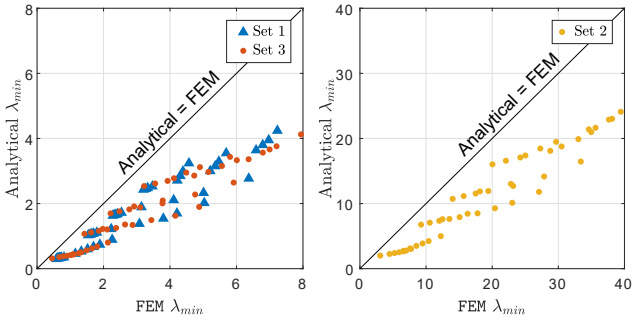

Figure 13: FEM/analytical method comparison

As mentioned above for the plain sphere, the non linear analyses are useful to evaluate the performance of shells subjected to high external pressure, in particular when the collapse is considered. However, because of the high computational cost, this type of analysis can be hardly used in the design or optimization phase.

3.7 Manufacturing techniques

In the case of metallic geodesic domes, the complexity of the ribbing limits the manufacturing techniques to few solutions. In [25], aluminum domes were obtained by hand routing machining from thick domes pre-formed by hot spinning and bakelite geodesic domes were fabricated from plastic sheets pressure formed into spherical shells, on which ribs were bonded. Machining geodesic domes requires 5-axis machines and small tools, resulting in high costs and long fabrication time, especially in case of hard materials, such as titanium alloys.

These manufacturing issues can be more easily addressed by switching to Additive Manufacturing (AM) techniques. In fact, AM allows to fabricate complex geometries, resulting in improved performance and mass savings, especially when coupled with optimization tools [31], or in integrated systems, where assemblies are fabricated in one single process. Moreover, AM processes are in general characterized by reduced lead time and costs, especially for small lots, making AM particularly suited for prototyping or customized products [32]. Many processes and materials are available today, or under development, ranging from polymers, to metals, to composites; in the case of metal additive manufacturing, the most common processes use powder bed fusion technologies, such as Electron Beam Melting or Selective Laser Melting [33]. Examples of isogrid stiffened panels or cylindrical shells fabricated by AM can be found in literature, especially for polymeric materials, such as PVC [34] or carbon fiber reinforced polymers [27, 28]. An hybrid fabrication technique was used in [29] to build an isogrid-stiffened patch antenna. A model of an isogrid reinforced mirror is presented in [30]; AM and a gradient alloy were used, having the surface of the mirror made of Invar and the ribs made of steel.

Considering geodesic domes and metal powder bed processes, two different fabrication directions are possible, as shown in Figure 14. However, support structures in the internal surface can be difficult to remove and could results in high surface roughness and irregularities. For this reason, layout B is recommended. Supports are needed at the base and in correspondence to the flange of the component. Post-machining of the external surface can be performed, to reduce the surface roughness. Some overhangs are still present in the upper part of the component; in order to avoid extra supports, chamfers can be added. Fillets can be used as well, to reduce stress concentration and crack initiations.

It must be noted that the analytical formulations previously described use isotropic material models, while the mechanical properties of Additively Manufactured materials can be not isotropic, due to the directionality of the process, especially when components are in the as-built condition. However, in the case analyzed here, components are usually subjected to heat treatments at high temperatures, which have beneficial effects, also reducing the anisotropy [35, 36]. For this reason, isotropic material properties can be considered, at least in the concept design phase; more detailed material models can be used for the verification of the final configuration of structure.

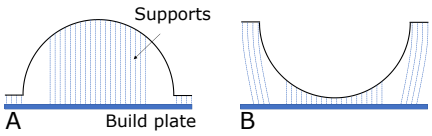

Figure 14: Printing directions and supports

4 Spherical planetary probes

Venus, Europa and Enceladus are potential targets for future robotic space missions. They are all characterized by harsh environmental conditions and, in particular, by high external pressure; hence, probes for in-situ exploration need robust vessels. If concepts of potential probes for Ocean World exploration are mainly cylindrical shells [1], spherical layouts are the most common solution for Venus landers [23, 37, 38], as they minimize the surface area exposed to the very high temperature of the environment (462°C).

In the early design stage, the external pressure due to Venus' environment is considered as the most severe loading condition. At first, the effects of the high temperature on the structural behavior can be neglected as well, as it is mitigated by the thermal control system. So, thermal expansion is not considered and material properties at room temperature are used. Past landing missions to Venus (Pioneer Venus, Venera probes) used plain, thick spherical shells, as shown in Figure 15. Several solutions of primary structures have been proposed over the years, assessing different materials and fabrication techniques [23], as well as different layouts, including internally pressurized tanks [38].

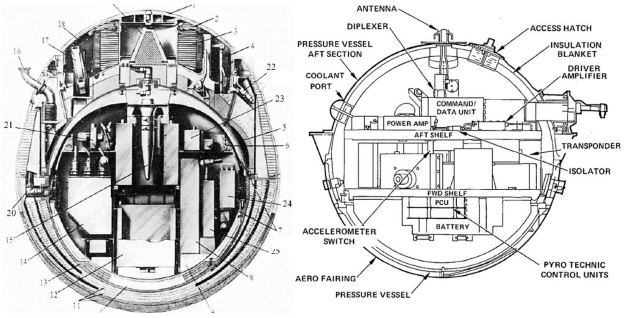

Figure 15: Venera 5 (left) and Pioneer Venus - Large probe (right) cutaway, adapted from [23, 40]

Geodesic domes and Additive Manufacturing have been investigated in [39]. A full-scale isogrid shell was designed, considering the design method described in the previous sections. Then, an experimental campaign was

performed on sub-scale components, to investigate the behavior of Additively Manufactured plain and isogrid shells and to assess the validity of the models (Figure 16). ⌀ 200 mm Ti6Al4V geodesic domes were designed according to the analytical method and considering the technology limitations related to the dimension of the powder bed of the AM machine and the accuracy of the process. The geometry was refined, adding fillets and chamfers to improve the manufacturability. Then, Finite Element Analysis was performed, using linear and non linear analyses, to predict the structural behavior and the failure pressure. Once the domes had been fabricated by Direct Metal Laser Sintering and the supports had been removed by machining, three geodesic domes and one plain dome were tested under hydrostatic pressure loading. In the case of the goedesic domes, repeatable failure modes were observed and the non-linear simulations were found consistent with the experimental results, with an error of 9%. Moreover, comparing the experimental failure pressure to the prediction made by the finite element linear analysis, the resulting knockdown factor was 44%, while the recommended factor for plain shells is about 30%. This suggests that geodesic domes are more robust and less sensitive to imperfections.

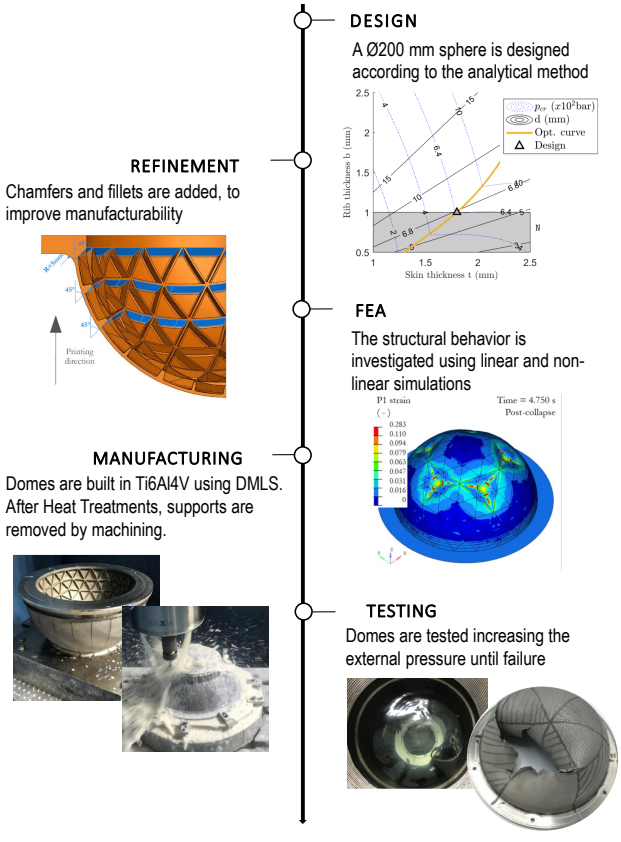

Figure 16: Experimental testing of sub-scale components [39]

5 Conclusions

The technical problem addressed here is the early design of primary structures of probes for the exploration of harsh environments. This kind of structures must be resistant to extreme pressures, but also lightweight, to meet the mission requirements. The tentative solution proposed here is to combine an isogrid-stiffening layout to Additive Manufacturing technologies. However, the complexity of the geometry, together with the non-linearities and the uncertainties typical of shell buckling, requires a modeling that starts from analytical approaches, uses numerical simulations and requires an optimization phase. The paper reports an analytical method for modeling the behavior of geodesic domes under external pressure loading, showing the feasibility of an optimization method based mainly on the balanced buckling modes. The feasibility of the integration of the isogrid and AM has been discussed as well, describing issues and potential benefits. A design path has been proposed, composed by different steps: the optimization of the isogrid layout, using the analytical method, the refinement of the geometry to improve the manufacturability, and the numerical simulations, to predict the failure pressure. An experimental campaign on Ti6Al4V domes was performed and showed promising results. Further experiments should be performed, to better assess the knockdown factor for geodesic domes and to investigate the sensitivity of the buckling modes to the isogrid parameters.

Acknowledgement: The authors gratefully acknowledge Eric Sunada for his guidance, Morgan Hendry for the support in the analytical design, and John Paul Borgonia for the support for the manufacturing topics (Jet Propulsion Laboratory, California Institute of Technology).

Conflict of Interests: The authors declare no conflict of interest regarding the publication of this paper.

References

[1] Fleurial J. et al., Notional Concept of Operations and System Capability Definition for Enabling Scientific Ocean Access Missions on Icy Worlds, EPSC-DPS Joint Meeting 2019 (15-20 September 2019, Geneva, Switzerland), 2019, 13

[2] Cutts J.A., Balint T.S., Chassefiere E., Kolawa E.A., Technology Perspectives in the Future Exploration of Venus In: L.W. Esposito, E.R. Stofan and T.E. Cravens (Ed.), Exploring Venus as a Terrestrial Planet, John Wiley & Sons, 2013
[3] Chu H.Y., The Evolution of the Fuller Geodesic Dome: From Black Mountain to Drop City, Des. Cult., 2018, 10, 121-137
[4] Metlen T.T., Palazotto A.N., Design of a Structure that Achieves Positive Buoyancy in Air Using a Vacuum, In: 54th AIAA/ASME/ASCE/AHS/ASC Structures, Structural Dynamics, and Materials Conference, (8-11 April 2013, Boston, MA, USA), 2013, 1881
[5] Adorno-Rodriguez R., Palazotto A.N., Nonlinear Structural Analysis of an Icosahedron Under an Internal Vacuum, J Aircraft, 2015, 52 (3), 878-883
[6] Khan A., Liquan W., Gang W., Imran M., Waqas H.M., Zaidi A.A., Concept Design of the Underwater Manned Seabed Walking Robot, J. Mar. Sci. Eng., 2019, 7 (10), 366
[7] Meschini A., Ridolfi A., Gelli J., Pagliai M., Rindi A., Pressure Hull Design Methods for Unmanned Underwater Vehicles, J. Mar. Sci. Eng., 2019, 7 (11), 382
[8] Zhang J., Zhang M., Cui W., Tang W., Wang F., Pan B., Elastic-plastic buckling of deep sea spherical pressure hulls, Mar. Struct., 2018, 57, 38–51
[9] Zhang Y.L., Jin J., Hou H.L., Liu S.Y., Wei X.L., The buckling strength of plexiglass protective shield under static water pressure, Eng. Fail. Anal., 2019, 99, 169-179
[10] Dini G., Princi E., Gamberini S., Gamberini L., Nemo's Garden: Growing plants underwater, In: Oceans 2016 MTS/IEEE Monterey, (2016, Monterey, CA), 2016, 1-6
[11] Bushnell D., Computerized buckling analysis of shells, Springer Science & Business Media, 2012
[12] Lee A., López Jiménez F., Marthelot J., Hutchinson J. W., Reis P.M., The Geometric Role of Precisely Engineered Imperfections on the Critical Buckling Load of Spherical Elastic Shells, J. Appl. Mech., 2016, 83 (11), 111005
[13] Wagner H.N.R., Sosa E. M., Ludwig T., Croll J.G.A., Hühne C., Robust design of imperfection sensitive thin-walled shells under axial compression, bending or external pressure, Int. J. Mech. Sci., 2019, 156, 205-220
[14] NASA SP-8032, Buckling of Thin-Walled Doubly curved shells, 1969
[15] Young W.C., Budnyas R.G., Roark's formulas for stress and strain, McGraw-Hill, New York, 2002
[16] Pan B.B., Cui W.C., Shen Y.S., Experimental verification of the new ultimate strength equation of spherical pressure hulls, Mar. Struct., 2012, 29(1), 269-176
[17] Evkin A.Y., Lykhachova O.V., Energy barrier as a criterion for stability estimation of spherical shell under uniform external pressure, Int. J. Solids Struct., 2017, 118-119, 14-23
[18] Zhang J., Huang C., Wagner H.N.R, Cui W., Tang W., Study on dented hemispheres under external hydrostatic pressure, Mar. Struct., 2020, 74, 102819
[19] Rotter J.M., Shell buckling design and assessment and the LBA-MNA methodology, Stahlbau, 2011, 80 (11)
[20] EN 1993-1-6, Eurocode 3: Design of steel structures, 1-6, Tech. rep., Comité Européen de Normalisation, 2007
[21] Pranesh S.B., Kumar D., Subramanian V.A., Sathianarayanan D., Ramadass G.A., Non-linear buckling analysis of imperfect thin spherical pressure hull for manned submersible, J. Ocean. Eng. Sci., 2017, 2 (4), 293-300
[22] Tall M., Hariri S., Le Grognec P., Simonet Y., Elastoplastic buckling and collapse of spherical shells under combined loadings, Thin-Walled Struct., 2018, 123, 114-125
[23] Pauken M., Kolawa E., Manvi R., Sokolowski W., Lewis J., Pressure Vessel Technology Developments, In: 4th International Planetary Probe Workshop, (27-30 June 2006, Pasadena, California, USA), 2006
[24] Bellini C., Sorrentino L., Characterization of Isogrid Structure in GFRP, Frattura ed Integrità Strutturale, 2018, 46, 319-331
[25] NASA-CR-62257 Determination of minimum weight shape and stiffening configuration for doubly curved shells subjected to external buckling pressures, 1964
[26] NASA CR-124075, Isogrid design handbook, 1973
[27] Forcellese A.,Di Pompeo V., Simoncini M., Vita A., Manufacturing of Isogrid Composite Structures by 3D Printing, Procedia Manufacturing, 2020, 47, 1096-1100
[28] Junqueira D.M., Gomes G.F., Silveira M.E., Ancelotti A.C., Design Optimization and Development of Tubular Isogrid Composites Tubes for Lower Limb Prosthesis, Appl Compos Mater, 2019, 26, 273–297
[29] MacDonald E. et al., Fabricating patch antennas within complex dielectric structures through multi-process 3D printing, J Manuf Process, 2018, 34 A, 197-203
[30] Hofmann D.C., et al., Compositionally graded metals: A new frontier of additive manufacturing, J Mater Res, 2014, 29.17, 1899-1910.
[31] Brusa E., Sesana R., Ossola E., Numerical modeling and testing of mechanical behavior of AM Titanium alloy bracket for aerospace applications, Proc. Struct. Integrity, 2017, 5, 753-760
[32] Brischetto S., Ciano A., Ferro C.G., A multipurpose modular drone with adjustable arms produced via the FDM additive manufacturing process, Curved and Layer. Struct., 2016, 3, 202-213
[33] Razavykia A., Brusa E., Delprete C., Yavari R.,n Overview of Additive Manufacturing Technologies-A Review to Technical Synthesis in Numerical Study of Selective Laser Melting, Materials, 2020, 13 (17), 3895
[34] Li M., Lai C., Zheng Q., Han B., Wu H., Fan H., Design and mechanical properties of hierarchical isogrid structures validated by 3D printing technique, Mater Design, 2019, 168, 107664
[35] Cain V., Thijs L., Van Humbeeck J., Van Hooreweder B., Knutsen R., Crack propagation and fracture toughness of Ti6Al4V alloy produced by selective laser melting, Additive Manufacturing, 2015, 5, 68-76
[36] Y. Kok, Anisotropy and heterogeneity of microstructure and mechanical properties in metal additive manufacturing: A critical review, Mater Design, 2018, 139, 565-586, DOI:10.1016/j.matdes.2017.11.021
[37] Hall J.L., MacNeal P.D., Salama M.A., Jones J.A., Heun M.K., Thermal and Structural Test Results for a Venus Deep-Atmosphere Instrument Enclosure, J. Spacecraft Rockets, 2000, 37, 142-144
[38] Bugby D., Seghi S., Kroliczek E., Pauken M., Novel Architecture for a Long-Life, Lightweight Venus Lander, AIP Conference Proceedings, 2009, 1103, 39
[39] Ossola E., Borgonia J.P., Hendry M., Sunada E., Brusa E., Sesana R., Design of Isogrid Shells for Venus Surface Probes, J Spacecraft and Rockets, (in press)
[40] Fimmel R.O., Colin L., Burgess E., Pioneer Venus, NASA Spec. Publ., NASA SP-461, 1983